Chapter II:
Milky Way and M31

New Dimensions of Galactic Chemical Evolution

David H. Weinberg

Department of Astronomy and CCAPP, Ohio State University,
140 W. 18th Ave., Columbus, OH 43210, USA. email: weinberg.21@osu.edu

Abstract. Dramatic recent progress in understanding galactic chemical evolution (GCE) has been driven partly by direct observations of the distant past with *HST* and *JWST* and partly by archaeological interpretation of stellar abundances from giant high-resolution spectroscopic surveys (APOGEE, GALAH) and the complementary power of *Gaia* astrometry and photometry. Focusing on archaeology, I give a rapid-fire, and I hope synthesizing, review of work my collaborators and I have done on theoretical modeling and observational interpretation. I discuss (1) the interleaved but distinguishable roles of stellar scale astrophysics and galactic scale astrophysics in governing GCE, (2) the use of abundance ratio trends to empirically infer nucleosynthetic yields, (3) the uncertainty in the overall scale of yields and its degeneracy with the importance of galactic outflows, (4) the emergence of equilibrium in GCE, (5) the dimensionality of the stellar distribution in chemical abundance space, and (6) insights from chemical abundances on the early history of the Milky Way, including measurements of the intrinsic scatter of abundance ratios in metal-poor stars ($-2 \leq$ [Fe/H] ≤ -1) suggesting that a typical halo star at this metallicity is enriched by the products of $N \sim 50$ supernovae mixed over $\sim 10^5 M_\odot$ of star-forming gas.

Keywords. Galaxy: abundances – Galaxy: evolution – galaxies: abundances – galaxies: evolution

1. Introduction

I am a relative latecomer to the field of galactic chemical evolution (GCE), after working on large scale structure and other aspects of galaxy formation through most of my career. This late arrival has advantages and disadvantages. The principal advantage is fresh perspective informed by my experience in other fields. The principal disadvantage is my sometimes limited knowledge of what has come before, which in a voluminous field like GCE is a lot (e.g., Tinsley 1980, Prantzos & Aubert 1995, Pagel 1997, Kobayashi et al. 2006, Matteucci 2012). Fortunately, I have had wonderful collaborators to help mitigate my ignorance. Even more fortunately, dramatic advances in GCE data sets have created radically new opportunities for modeling and interpretation. For me personally, the APOGEE survey (Majewski et al. 2017) of SDSS-III (Eisenstein et al. 2011), SDSS-IV (Blanton et al. 2017), and SDSS-V (Kollmeier et al. 2017) has been most important, but similar advances are coming from GALAH (Buder et al. 2021), *Gaia* (Gaia Collaboration et al. 2023), SEGUE (Yanny et al. 2013, Rockosi et al. 2022), LAMOST (Luo et al. 2015), H3 (Conroy et al. 2019), and numerous observing programs that target specific stellar populations in the Milky Way and its neighbors.

It is a long time since I wrote a conference proceedings, but IAU Symposia have always been the gold standard of these, and this is my first opportunity to contribute to one! As in my talk, I will use this opportunity to run lightly over a lot of ground, and to

Table 1. A partial list of abbreviations used.

Abbreviation	Meaning
AGB	asymptotic giant branch
CCSN	core collapse supernova(e)
DTD	delay time distribution
GCE	galactic chemical evolution
GSA	galactic scale astrophysics
IMF	initial mass function
ISM	interstellar medium
SFE	star formation efficiency
SFH	star formation history
SFR	star formation rate
SNIa	Type Ia supernova (e)
SSA	stellar scale astrophysics

make editorial comments I might never get past a stern journal referee. A partial list of abbreviations used is given in Table 1.

2. The Structure of the GCE Problem

A GCE model relies on "stellar scale" astrophysics that determines the IMF-averaged yields and delay time distribution (DTD) of different enrichment channels, and on "galactic scale" astrophysics such as accretion and star formation history, star formation laws, outflows, radial gas flows, and redistribution of stars by radial migration, disk heating, and mergers. For compactness, I will refer to these components as SSA and GSA, respectively. Distinct GCE models may differ in their SSA assumptions, their GSA assumptions, or both. Model predictions can be tested against a wide range of observables in the Milky Way and other galaxies, including abundance ratio trends (e.g., $[\alpha/\text{Fe}]$ vs. $[\text{Fe/H}]$), distribution functions (e.g., $p([\text{Fe/H}])$, $p([\alpha/\text{Fe}])$), and the dependence of these on a stellar population's age, galactic position, and kinematics.

This structure is reminiscent (to this reminiscer, anyway) of galaxy formation in the late '80s and early '90s. Models depended both on poorly known cosmological inputs — such as Ω_m, Ω_b, the primordial power spectrum, and the nature of dark matter — and on galactic scale modeling of gas cooling, angular momentum, feedback, outflows, mergers, and so forth. They could be tested against observations of galaxy clustering and galaxy properties over a range of redshifts, and the interesting challenge was to learn about *both* cosmology and galaxy scale physics despite the tradeoffs between the two.

If nucleosythetic yields were a solved theoretical problem, then our GCE models could take them as robust inputs and focus on constraining GSA — rather like galaxy formation today, where the uncertainties in cosmological parameters are mostly negligible compared to the uncertainties in "gastrophysics." However, the physics challenges of nucleosynthesis calculations and the variance of predictions from study to study are large enough that I usually take these predictions as "serving suggestions" rather than recipes to be followed to the letter.

In GCE, one thing my collaborators and I have tried to do is to separate constraints on SSA and GSA by drawing on complementary observables. Loosely speaking (see, e.g., Andrews et al. 2017, Weinberg et al. 2017), models predict that abundance ratio trends depend most strongly on yields (SSA), while distribution functions depend on star formation history (SFH), stellar radial migration (Schönrich & Binney 2009, Hayden et al. 2015, Loebman et al. 2016, Johnson et al. 2021), and other GSA.

APOGEE abundances show that the median trends of $[\text{X/Mg}]$ vs. $[\text{Mg/H}]$ are nearly universal throughout the Milky Way disk (Weinberg et al. 2019) and bulge (Griffith et al.

2021a), provided one separately examines the high-α and low-α populations. This universality directly demonstrates the dominant role of SSA in determining these trends, since GSA features like SFH and gas flows are almost certainly different between the outer disk, inner disk, and bulge. Mg is a better reference element than Fe for this purpose because it has a single astrophysical source, massive stars exploding as core collapse supernovae (CCSN), whereas Fe comes from both CCSN and Type Ia supernovae (SNIa). The separation between high-α and low-α populations is really caused by the difference in Fe from SNIa, not by differences in α elements themselves. For other elements, the separation of the two [X/Mg] sequences depends on the relative contribution of CCSN (or, more generally, prompt sources) vs. SNIa (or, more generally, delayed sources) to element X. By formalizing this idea in a "2-process model," we have used observed trends in APOGEE and GALAH to derive empirical constraints on the IMF-averaged yields of CCSN and SNIa for many elements (Weinberg et al. 2019, 2022, Griffith et al. 2019, 2022). For elements in which the delayed contribution comes from asymptotic giant branch (AGB) stars rather than SNIa, this decomposition is only approximate. Isolating CCSN yields from other contributions enables sharper tests of theoretical models of CCSN and black hole formation (Griffith et al. 2021b).

In a related vein, Johnson et al. (2023) exploit the dependence of abundance ratios on SSA to derive empirical constraints on the metallicity dependence of nitrogen yields from the trend of [N/O] vs. [O/H] observed in the Milky Way and external galaxies. Separating the contributions of massive stars and intermediate mass stars to the IMF-averaged yield is trickier, but we show that one can get useful empirical constraints on this decomposition from the separation of [N/O] ratios between high-α and low-α stellar populations in the Milky Way disk (Vincenzo et al. 2021; J. Roberts et al., in prep.).

One key difference between present-day GCE and early '90s galaxy formation is that abundance "measurements" are themselves derived by fitting intricate stellar atmosphere models to observed spectra, making them subject to complex theoretical and observational systematics. Therefore, when deducing lessons about chemical evolution from abundance data, one must also allow for the possibility of observational systematics that are comparable in magnitude to GCE model differences. One important example is the difference between [O/Fe] or [O/Mg] trends found in optical vs. near-IR spectroscopic surveys (Griffith et al. 2019, 2022), or even between analyses of the same near-IR spectra that adopt different $T_{\rm eff}$ and $\log g$ calibrations (Hayes et al. 2022). IMF-averaged CCSN yield models predict that [O/Mg] is nearly independent of metallicity (Andrews et al. 2017), as found in APOGEE. If the sloped [O/Mg] trend found in optical surveys is correct, it has sharp implications for the origin of O, Mg, or both.

3. Yields, Outflows, and Equilibrium

While abundance ratios provide a powerful tool for constraining yields, or more generally SSA, with little sensitivity to galactic scale uncertainties, there is a critical degeneracy between the overall scale of yields and the mass-loading factor $\eta \equiv \dot{M}_{\rm out}/\dot{M}_*$ of galactic outflows. This degeneracy can be easily understood in one-zone GCE models, which assume a fully mixed gas reservoir so that the abundances of newly forming stars depend on time but not on spatial position. These models have a long history (e.g., Talbot & Arnett 1971, Larson 1972). Here I summarize some of the lessons from the analytic solutions of Weinberg et al. (2017, hereafter WAF).

For an element like O (or Mg) whose production is dominated by massive stars, one can approximate enrichment as instantaneous with a net IMF-averaged yield $y_{\rm O}^{\rm cc}$ that includes CCSN and massive star winds. The evolution of oxygen mass in the gas reservoir follows

$$\dot{M}_{\rm O} = y_{\rm O}^{\rm cc} \dot{M}_* - Z_{\rm O} \dot{M}_* - \eta Z_{\rm O} \dot{M}_* + r Z_{\rm O} \dot{M}_* \qquad (3.1)$$

$$= y_{\rm O}^{\rm cc} \dot{M}_* - (1 + \eta - r) \dot{M}_* Z_{\rm O} \ . \qquad (3.2)$$

Here $Z_O = M_O/M_g$ is the oxygen mass fraction of the ISM, and the terms on the r.h.s. represent new O production, loss of O from the ISM to star formation and outflow, and return of O to the ISM by recycling of stellar envelopes. Although some recycling comes from lower mass stars with long lifetimes, approximating it as instantaneous is usually accurate compared to calculations that include full time dependence. For a Kroupa (2001) IMF, the recycling factor $r \approx 0.4$, roughly half of it from stars with $M > 8M_\odot$.

As first argued by Larson (1972), if there is ongoing gas accretion that sustains star formation, then the ISM abundance does not grow indefinitely but instead reaches an equilibrium when the source and sink terms of Eq. 3.2 balance. For an exponential star formation history, $\dot{M}_* \propto e^{-t/\tau_{\rm sfh}}$, and a time-independent star formation *efficiency*, SFE $= \tau_*^{-1} = \dot{M}_*/M_g$, one can show that the equilibrium abundance is

$$Z_{\rm O,eq} = \frac{y_O^{\rm cc}}{1 + \eta - r - \tau_*/\tau_{\rm sfh}} \ . \tag{3.3}$$

The full time-dependence is

$$Z_O(t) = Z_{\rm O,eq} \left(1 - e^{-t/\bar{\tau}}\right) \tag{3.4}$$

with

$$\bar{\tau} = \frac{\tau_*}{1 + \eta - r - \tau_*/\tau_{\rm sfh}} \ . \tag{3.5}$$

In the molecular gas of present-day star forming galaxies a typical SFE timescale is $\tau_* \approx 2\,{\rm Gyr}$ (Leroy et al. 2008, Sun et al. 2023), so the correction $\tau_*/\tau_{\rm sfh}$ is often small compared to $1 + \eta - r$.

Importantly, one can also find analytic solutions for Fe enrichment by SNIa if one approximates the DTD as $R_{\rm Ia}(t) \propto e^{-(t-t_d)/\tau_{\rm Ia}}$ after a minimum delay time t_d (equation 53 of WAF), which allows one to calculate the evolution of [α/Fe] and [Fe/H] for realistic cases. The introduction of the new timescale $\tau_{\rm Ia}$ makes the solutions more complex than Eq. 3.4, but the behavior remains intuitive. One can accurately approximate a $t^{-1.1}$ power-law DTD (Maoz & Graur 2017) as a sum of two exponentials, and the presence of short-$\tau_{\rm Ia}$ and long-$\tau_{\rm Ia}$ components leads to interesting behavior in some scenarios. WAF also present analytic solutions for a linear exponential SFH, $\dot{M}_* \propto te^{-t/\tau_{\rm sfh}}$, and for cases with sudden changes of η or τ_*, and their equation (117) provides a general way to model more complex star formation histories by combining the solutions for exponential histories.

For understanding the yield-outflow degeneracy, equations 3-5 convey the key points. The ISM abundance in equilibrium depends on $y_O^{\rm cc}$ *and* η because the latter controls the rate at which metals are lost in galactic winds. The timescale $\bar{\tau}$ for approaching equilibrium is typically short compared to the age of the galaxy, though it can become long if η is small and star formation is inefficient.

For a Kroupa IMF and the CCSN yields of Chieffi & Limongi (2004) and Limongi & Chieffi (2006), the predicted yield is $y_O^{\rm cc} \approx 0.015$ (i.e., $1.5M_\odot$ of oxygen produced per $100M_\odot$ of stars formed). Achieving solar oxygen abundance $Z_{\rm O,\odot} \approx 0.006$ (Asplund et al. 2009) therefore requires strong outflows, with $\eta \approx 2$, a long-standing result in theoretical models of the mass-metallicity relation (e.g., Finlator & Davé 2008, Peeples & Shankar 2011, Zahid et al. 2012) as well as my group's GCE models (e.g., Andrews et al. 2017, WAF, Johnson et al. 2021). I was initially puzzled that the "Trieste group" (which by now spans many nations) was able to produce successful GCE models with no outflows (e.g., Chiappini, Matteucci, & Gratton 1997, Matteucci & François 1989, Minchev et al. 2013, Spitoni et al. 2019), but I eventually learned it is because they adopt an IMF-averaged O yield that is about $3\times$ lower than mine, with $y_O^{\rm cc} \approx Z_{\rm O,\odot}$ (Minchev, private communication). In their case, the principal reason for this much lower
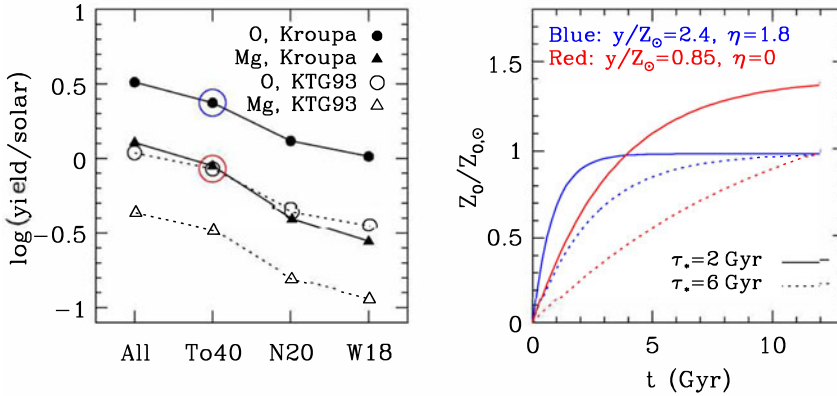
Figure 1. (Left) IMF-averaged net yield of O (circles) or Mg (triangles) computed from the CCSN models of Griffith et al. (2021b) for a Kroupa (2001) IMF (solid) or a Kroupa et al. (1993) IMF (dotted), with four scenarios for black hole formation: all stars born with $8M_\odot \leq M \leq 120M_\odot$ explode as CCSN; stars with $8M_\odot \leq M \leq 40M_\odot$ explode; or the explosion landscapes predicted by Sukhbold et al. (2016) for two different neutrino-driven central engines. Yields are scaled to the corresponding solar abundance. For the same black hole scenario the predicted yields of the two IMFs differ by a factor of three. For a given IMF, the difference between the scenarios with the most or least black hole formation is also a factor of three. (Right) Evolution of the O abundance for the yields marked by the blue and red circle in the left-hand panel, $y_O^{cc}/Z_{O,\odot} = 2.4$ and 0.85, respectively, with correspondingly chosen outflow mass loading factors $\eta = 1.8$ or $\eta = 0$. Solid curves use an SFE timescale $\tau_* = 2\,\mathrm{Gyr}$ typical of molecular gas in local galaxies, while dotted curves use a longer SFE timescale $\tau_* = 6\,\mathrm{Gyr}$. All curves use the analytic solution (Eq. 3.4) for an exponential SFH and assume $\tau_{\mathrm{sfh}} \to \infty$ (constant SFR).

yield is the assumption of a steeper IMF (Miller & Scalo 1979, Kroupa et al. 1993), with $\phi(M) \propto M^{-2.7}$ at high masses compared to $M^{-2.3}$ for a Kroupa (2001) IMF.

In addition to the IMF, a key source of uncertainty in CCSN yields is black hole formation (Sukhbold et al. 2016; Griffith et al. 2021b). Production of O, Mg, and other α-elements grows rapidly with progenitor mass, but if the most massive stars implode to black holes then they never release these products to the ISM. The left panel of Fig. 1, adapted from Griffith et al. (2021b), shows their IMF-averaged O and Mg yields for a Kroupa (2001) IMF or the much steeper Kroupa et al. (1993) IMF, and for four different scenarios of black hole formation: the complex "landscapes" predicted for two neutrino-driven central engines (W18 and N20) by Sukhbold et al. (2016), a sharp transition from explosion to implosion at $M = 40M_\odot$, or no black hole formation. For a given IMF, the yields predicted for these four scenarios span a factor of three, and for a given black hole scenario the difference between these two IMFs is also a factor of three.

The right panel of Fig. 1 shows $Z_O(t)$ from Eq. 3.4 for two different combinations of yield and η: $y_O^{cc}/Z_{O,\odot} = 2.4$ and $\eta = 1.8$ (blue) and $y_O^{cc}/Z_{O,\odot} = 0.85$ and $\eta = 0$ (red). In each case we assume constant SFR ($\tau_{\mathrm{sfh}} \to \infty$) and $\tau_* = 2\,\mathrm{Gyr}$ (solid) or $6\,\mathrm{Gyr}$ (dotted). As expected, both the high-yield/high-η and low-yield/low-η combinations can produce $Z_O \approx Z_{O,\odot}$ at late times. These examples and Eq. 3.5 also explain why equilibrium is a central concept in my group's GCE models (and earlier work such as Finlator & Davé 2008, Davé et al. 2012) but is not nearly so evident in the Trieste models. If $\eta \approx 2$ then the timescale for reaching equilibrium is fairly short, even with $\tau_* = 6\,\mathrm{Gyr}$ (blue dotted line). If $\eta = 0$ then the timescale is longer, and Z_O may still be climbing at $t = 10 - 13\,\mathrm{Gyr}$. For the $\eta = 0$, $\tau_* = 6\,\mathrm{Gyr}$ model (red dotted line), the abundance remains well below equilibrium even at $t = 12\,\mathrm{Gyr}$. The impact of η and τ_* on time-evolution is amplified for Fe because of the delayed SNIa contribution.

The scale of yields is therefore tightly connected to the importance of outflows *and* the emergence of equilibrium. Unfortunately, black hole formation and other theoretical uncertainties make it difficult to predict the absolute scale of CCSN yields with confidence. Deuterium is one possible way forward because its theoretical yield is perfectly known: stars destroy whatever D they are born with, making $y_D = 0$ (all deuterium is primordial). Unfortunately, the large sightline-to-sightline variance of D/H (Linsky et al. 2006), plausibly interpreted as a sign of dust depletion onto PAH molecules, makes determining the intrinsic ISM D/H ratio difficult. For the ISM D/H value advocated by Linsky et al. (2006), the implied values of η and y_O^{cc} are fairly high, similar to the blue models in Fig. 1 (Weinberg 2017). The mean Fe yield of CCSN (Rodríguez et al. 2022) offers another, empirical route towards determining the overall yield scale (Weinberg, in prep.). There are uncertainties in going from the measured quantity to α-element yields such as y_O^{cc}, but the Rodriguez et al. measurement suggests a value intermediate between the two cases shown in Fig. 1, requiring mild outflows ($\eta \approx 1$) to reach solar abundance.

4. Dimensionality and Scatter

Despite the yield-outflow degeneracy, abundance ratio trends (e.g., [X/Mg] vs. [Mg/H]) provide strong empirical constraints on yield *ratios*, and by exploiting the separation of high-α and low-α populations one can start to separate the contribution of distinct astrophysical processes (e.g., CCSN vs. SNIa vs. AGB). The addition of stellar ages — from asteroseismology, or parallax + photometry, or spectroscopic diagnostics trained on these methods — helps further separate prompt and delayed enrichment channels and provides leverage on SFE and SFH. Models with different SFH but the same yields and SFE produce similar abundance ratio tracks, but they produce different metallicity distribution functions because the number of stars formed at a given metallicity is proportional to the SFR. By fitting one-zone models to stellar abundances of dwarf spheroidals or stellar streams one can get interesting SFH constraints from the metallicity distribution alone (Sandford et al. 2022), and these become sharper and more robust if the data include [α/Fe] ratios and stellar ages (Johnson et al. 2021).

With large, homogeneous data sets, one can measure the *scatter* around mean abundance trends to gain additional diagnostics of yields, enrichment history, mixing of stellar populations by mergers or migration, and mixing of metals within the star-forming ISM. Measuring intrinsic scatter accurately is challenging because one must carefully assess the observational contribution, including scatter caused by differential abundance systematics across the stellar sample.

Scatter in the high-dimensional space of stellar abundance ratios is a nuanced concept, linked to the dimensionality of the stellar distribution in this space. One of the earliest investigations of this dimensionality was led by Yuan-Sen Ting, who showed that 6-9 principal components were required to explain the abundance distribution of available high-resolution data sets (Ting et al. 2012; for related approaches see Andrews et al. 2012, 2017 and Patil et al. 2022). The dimensionality of the distribution is connected to the number of distinct processes that contribute to the observed abundances, but the connection is not a simple one. For example, in a one-zone model with a fully mixed gas reservoir, all stellar abundances depend on a single parameter (time) even if many enrichment channels are operating. To produce scatter one needs multiple enrichment channels and either imperfect ISM mixing (Krumholz & Ting 2018) or the mixing of stellar populations that experience different relative contributions from these channels.

The success of the 2-process model in fitting individual abundance patterns of Milky Way disk stars in APOGEE and GALAH shows that much of the star-to-star variation is explained by two components, one describing overall enrichment and a second describing the ratio of CCSN/SNIa enrichment (Weinberg et al. 2022; Griffith et al. 2022). Thus, to

a surprisingly good approximation one can predict all of a star's APOGEE or GALAH abundances from its [Mg/H] and [Mg/Fe] alone. In a similar fashion, one can predict these abundances to surprising accuracy from [Fe/H] and age (Ness et al. 2019). It would be interesting but ultimately disappointing if this 2-dimensional description were perfect.

Fortunately, it isn't. My collaborators and I have investigated this issue in two complementary ways, by examining the conditional distribution $p([X/Fe]|[Fe/H], [Mg/Fe])$ and its generalizations in APOGEE (Ting & Weinberg 2022) and by examining the residuals $\Delta([X/H])$ of stellar abundances relative to a 2-process fit in APOGEE and GALAH (Weinberg et al. 2022, Griffith et al. 2022). Each of these studies covers 15-16 elemental abundances. Key findings include:

(1) The observed total scatter (intrinsic + observational) around a 2-d fit for high-S/N APOGEE stars ranges from $\approx 0.01 - 0.02$ dex (Mg, O, Si, Ca, Fe, Ni) to ≈ 0.1 dex (Na, K, V, Ce), with a median of 0.03 dex.

(2) While inferring intrinsic scatter from total scatter requires precise knowledge of observational uncertainties, the correlation of abundance residuals provides robust evidence for additional dimensions in abundance space.

(3) One must condition on at least seven elements (e.g., Fe, Mg, O, Ni, Si, Ca, Al) before the residual correlations of remaining APOGEE elements are consistent with observational noise.

(4) Much of the [α/Fe] scatter *within* the high-α and low-α disk populations is caused by CCSN/SNIa variation within those populations at fixed [Fe/H]. These variations in turn are correlated with age.

(5) APOGEE 2-process residuals show correlations among Ca, Na, Al, K, Cr, and Ce and separately among Ni, V, Mn, and Co.

(6) GALAH 2-process residuals show correlations between Ba and Y, expected because both have large AGB s-process contributions, and significant correlations of these two with Zn.

(7) Ba and Y in GALAH and Ce in APOGEE show increasing positive residuals at young stellar ages, implying a late-time enhancement of AGB enrichment relative to SNIa enrichment. Intriguingly, Na shows a similar pattern in APOGEE even though it is not expected to have a large AGB contribution.

(8) Residual abundances provide a powerful method for comparing stellar populations, including dwarf satellites, streams, and star clusters, because they control for star-by-star differences in overall metallicity and [α/Fe] that can otherwise mask subtler differences in individual elements.

5. The Early History of the Milky Way

Much of the discussion above focuses on the regime of the Milky Way thin and thick disks. The defining principle of IAU 377 was to connect studies of the early Milky Way to those of high-redshift galaxies. I will conclude with three recent GCE studies of the early Milky Way, each of which I mentioned in my talk.

While searches for low metallicity stars have often focused on the nearby Galactic halo, theoretical models predict that the *oldest* stars should be concentrated near the center of the Galaxy (White & Springel 2000). Deriving metallicities from *Gaia* BP/RP spectra with a machine learning algorithm trained on APOGEE/*Gaia* overlap, Rix et al. (2022) show that stars with [M/H] < −1.5 are indeed centrally concentrated, with a Gaussian radial extent σ_R of only 2.7 kpc. Over the range $-2 \leq$ [M/H] ≤ -1 the observed metallicity distribution follows $d \log n/d$[M/H] = 1. In this regime, far below equilibrium, one can ignore the loss terms in Eq. 3.2 and derive a fairly general prediction
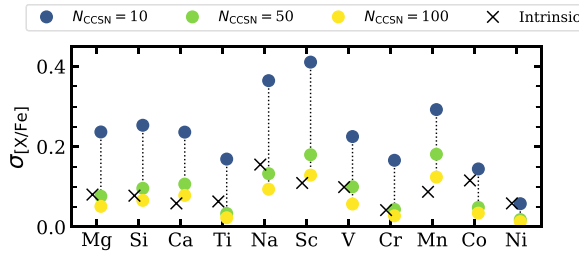
Figure 2. Crosses show the RMS intrinsic scatter in [X/Fe] at fixed [Fe/H] measured in a sample of 86 subgiant halo stars with $-2 \leq$ [Fe/H] ≤ -1. Circles show the RMS scatter predicted for random draws from the high-mass IMF producing $N = 10$ (blue), 50 (green), or 100 (yellow) CCSN, using the mass-dependent CCSN yields of Sukhbold et al. (2016). For most elements, the measured scatter corresponds to the predicted scatter for $N \approx 50$. From Griffith et al. (2023).

$$\frac{d \log n}{d[\text{M/H}]} = \left[1 - \left(\frac{M_*}{M_g}\right)\left(\frac{\tau_* \dot{M}_g}{M_g}\right)\right]^{-1} \tag{5.6}$$

The combination $(\tau_* \dot{M}_g / M_g)$ corresponds to the fractional change of the gas reservoir mass over one SFE timescale. The observed slope of unity matches the value theoretically expected for a small stellar mass fraction and/or a slowly changing gas reservoir.

APOGEE disk abundances show a plateau at [Mg/Fe] ≈ 0.35 for stars with $-1.2 \leq$ [Fe/H] ≤ -0.6, which is conventionally interpreted as representing the CCSN yield ratio. However, after using kinematic data to remove accreted halo stars, Conroy et al. (2022) find a more complex evolution in the H3 survey. For $-2.5 \leq$ [Fe/H] ≤ -1.5 the typical $[\alpha/\text{Fe}]$ declines from ≈ 0.6 to ≈ 0.3, then rises slightly for $-1.5 \leq$ [Fe/H] ≤ -0.5. With similar kinematic cuts, the APOGEE data are consistent with this behavior. Conroy et al. (2022) interpret this trend with a model in which the true CCSN plateau is at $[\alpha/\text{Fe}] \approx$ 0.6, the initial decline in $[\alpha/\text{Fe}]$ is caused by SNIa enrichment with a very low SFE ($\tau_* \approx 50\,\text{Gyr}$), and the rise in $[\alpha/\text{Fe}]$ for [Fe/H] > -1.5 is caused by rapidly accelerating SFE during which τ_* drops from 50 Gyr to 2 Gyr. This "simmer-to-boil" transition also coincides with a rapid increase in the angular momentum of stellar populations over the range $-1.5 <$ [Fe/H] < -0.9, also found in the analyses of Belokurov & Kravtsov (2022) and Rix et al. (2023). While there is still much to be decoded in these data, it appears that we are seeing both the kinematic and chemical birth of the Milky Way disk in these archaeological studies.

The scatter of disk star abundances around 2-process predictions is small, but we may reasonably expect scatter to be larger at low metallicities that probe early phases of chemical evolution. Griffith et al. (2023) measure abundances of 12 elements in 86 metal-poor subgiants ($-2 \leq$ [Fe/H] ≤ -1), with a survey strategy and analysis procedures designed specifically to allow robust determination of the intrinsic scatter. We find RMS intrinsic scatter in [X/Fe] at fixed [Fe/H] ranging from 0.04 dex (Cr) to 0.16 dex (Na), with a median of 0.08 dex. One plausible interpretation of this scatter is from stochastic sampling of the IMF, as any individual star is enriched not by the IMF-averaged CCSN yield but by the particular set of supernovae that enriched its birth environment.

The Griffith et al. measurements are well explained if the number of CCSN contributing to the enrichment of a given star is $N \sim 50$ (Fig. 2). The stochastic CCSN model roughly (though not perfectly) predicts the variation of scatter from element to element, and it also roughly explains the correlations of element fluctuations from star to star (fig. 15 of Griffith et al. 2023). Producing the median metallicity of the sample with $N = 50$ CCSN requires that the products of these CCSN be diluted by about $10^5 M_\odot$ of gas, orders of magnitude smaller than the likely mass of the Galaxy at this epoch. There are

factor-of-three level uncertainties in this argument, and even the basic interpretation of scatter as a stochastic IMF sampling effect may be incorrect. Nonetheless, this analysis illustrates what we can hope to learn by studying scatter around abundance trends as well as the trends themselves. If our stochastic sampling interpretation is correct, then the early Galaxy was divided into many ($10^4 - 10^6$) chemically disconnected regions, with each newly formed star sampling only the nucleosynthetic products of its own elemental horizon.

Acknowledgements

References

Andrews, B. H., Weinberg, D. H., Johnson, J. A., Bensby, T., & Feltzing, S. 2012, ActaA, 62, 269.

Andrews, B. H., Weinberg, D. H., Schönrich, R., & Johnson, J. A. 2017, ApJ, 835, 224

Asplund, M., Grevesse, N., Sauval, A. J., et al. 2009, ARA&A, 47, 481.

Belokurov, V. & Kravtsov, A. 2022, MNRAS, 514, 689.

Blanton, M. R., Bershady, M. A., Abolfathi, B., et al. 2017, AJ, 154, 28

Buder, S., Sharma, S., Kos, J., et al. 2021, MNRAS, 506, 150.

Chiappini, C., Matteucci, F., & Gratton, R. 1997, ApJ, 477, 765.

Chieffi, A. & Limongi, M. 2004, ApJ, 608, 405.

Conroy, C., Bonaca, A., Cargile, P., et al. 2019, ApJ, 883, 107.

Conroy, C., Weinberg, D. H., Naidu, R. P., et al. 2022, arXiv:2204.02989.

Davé, R., Finlator, K., & Oppenheimer, B. D. 2012, MNRAS, 421, 98.

Eisenstein, D. J., Weinberg, D. H., Agol, E., et al. 2011, AJ, 142, 72

Finlator, K. & Davé, R. 2008, MNRAS, 385, 2181.

Gaia Collaboration, Brown, A. G. A., Vallenari, A., et al. 2021, A&A, 649, A1.

Gaia Collaboration, Vallenari, A., Brown, A. G. A. et al. 2023, A&A, 674, A1

Griffith, E., Johnson, J. A., & Weinberg, D. H. 2019, ApJ, 886, 84

Griffith, E., Weinberg, D. H., Johnson, J. A., et al. 2021a, ApJ, 909, 77.

Griffith, E. J., Sukhbold, T., Weinberg, D. H., et al. 2021b, ApJ, 921, 73.

Griffith, E. J., Weinberg, D. H., Buder, S., et al. 2022, ApJ, 931, 23.

Griffith, E. J., Johnson, J. A., Weinberg, D. H., et al. 2023, ApJ, 944, 47.

Hayden, M. R., Bovy, J., Holtzman, J. A., et al. 2015, ApJ, 808, 132.

Hayes, C. R., Masseron, T., Sobeck, J., et al. 2022, ApJS, 262, 34.

Johnson, J. W., Weinberg, D. H., Vincenzo, F., et al. 2021, MNRAS, 508, 4484.

Johnson, J. W., Weinberg, D. H., Vincenzo, F., et al. 2023, MNRAS, 520, 782.

Kobayashi, C., Umeda, H., Nomoto, K., Tominaga, N., Ohkubo, T. 2006, ApJ, 653, 1145

Kollmeier, J. A., Zasowski, G., Rix, H.-W., et al. 2017, arXiv e-prints, arXiv:1711.03234.

Kroupa, P., Tout, C. A., & Gilmore, G. 1993, MNRAS, 262, 545.

Kroupa, P. 2001, MNRAS, 322, 231.

Krumholz, M. R. & Ting, Y.-S. 2018, MNRAS, 475, 2236.

Larson, R. B. 1972, Nature Physical Science, 236, 7.

Leroy, A. K., Walter, F., Brinks, E., et al. 2008, AJ, 136, 2782.

Limongi, M. & Chieffi, A. 2006, ApJ, 647, 483.

Linsky, J. L., Draine, B. T., Moos, H. W., et al. 2006, ApJ, 647, 1106.

Loebman, S. R., Debattista, V. P., Nidever, D. L., et al. 2016, ApJ, 818, L6.

Luo, A.-L., Zhao, Y.-H., Zhao, G. et al. 2015, RAA, 15, 1095

Majewski, S. R., Schiavon, R. P., Frinchaboy, P. M., et al. 2017, AJ, 154, 94.

Maoz, D. & Graur, O. 2017, ApJ, 848, 25.

Matteucci, F. & François, P. 1989, MNRAS, 239, 885

Matteucci, F. 2012, Chemical Evolution of Galaxies: Astronomy and Astrophysics Library. ISBN
    978-3-642-22490-4. Springer-Verlag Berlin Heidelberg, 2012.

Miller, G. E. & Scalo, J. M. 1979, ApJS, 41, 513.

Minchev, I., Chiappini, C., & Martig, M. 2013, A&A, 558, A9.

Ness, M. K., Johnston, K. V., Blancato, K., et al. 2019, ApJ, 883, 177.

Pagel, B. E. J. 1997, Nucleosynthesis and Chemical Evolution of Galaxies, by Bernard E. J.
    Pagel, pp. 392. ISBN 0521550610. Cambridge, UK: Cambridge University Press, October
    1997, 392

Patil, A. A., Bovy, J., Eadie, G., et al. 2022, ApJ, 926, 51.

Peeples, M. S. & Shankar, F. 2011, MNRAS, 417, 2962.

Prantzos, N. & Aubert, O. 1995, A&A, 302, 69

Rix, H.-W., Chandra, V., Andrae, R., et al. 2022, ApJ, 941, 45.

Rockosi, C. M., Lee, Y. S., Morrison, H. L., et al. 2022, ApJS, 259, 60.

Rodríguez, Ó., Maoz, D., & Nakar, E. 2022, arXiv:2209.05552.

Sandford, N. R., Weinberg, D. H., Weisz, D. R., et al. 2022, arXiv:2210.17045.

Schönrich, R., & Binney, J. 2009, MNRAS, 396, 203.

Spitoni, E., Silva Aguirre, V., Matteucci, F., et al. 2019, A&A, 623, A60.

Sukhbold, T., Ertl, T., Woosley, S. E., et al. 2016, ApJ, 821, 38.

Sun, J., Leroy, A. K., Ostriker, E. C., et al. 2023, ApJ, 945, L19.

Talbot, R. J. Jr. & Arnett, W. D. 1971, ApJ, 170, 409.

Ting, Y.-S., Freeman, K. C., Kobayashi, C., De Silva, G. M., & Bland-Hawthorn, J. 2012,
    MNRAS, 421, 1231.

Ting, Y.-S. & Weinberg, D. H. 2022, ApJ, 927, 209.

Tinsley, B. M. 1980, Fundamentals Cosmic Phys., 5, 287.

Vincenzo, F., Weinberg, D. H., Montalbán, J., et al. 2021, arXiv:2106.03912.

Weinberg, D. H. 2017, ApJ, 851, 25.

Weinberg, D. H., Andrews, B. H., & Freudenburg, J. 2017, ApJ, 837, 183.

Weinberg, D. H., Holtzman, J. A., Hasselquist, S., et al. 2019, ApJ, 874, 102.

Weinberg, D. H., Holtzman, J. A., Johnson, J. A., et al. 2022, ApJS, 260, 32.

White, S. D. M. & Springel, V. 2000, The First Stars, 327.

Yanny, B., Rockosi, C., Newberg, H. J., et al. 2009, AJ, 137, 4377.

Yanny, B. & Gardner, S. 2013, ApJ, 777, 91

Zahid, H. J., Dima, G. I., Kewley, L. J., Erb, D. K., Davé, R. 2012, ApJ, 757, 54